

Coarse grained modeling of self assembled DNA 3D structure using pragmatic soft ellipsoid contact potential

Abhirup Das and Jayashree Saha

Department of Physics, University of Calcutta, 92 Acharya Prafulla Chandra Road, Kolkata 700009

(Dated: February 10, 2026)

In this paper, we present a coarse-grained model of DNA based on the soft ellipsoid contact potential (ECP) to evaluate the base pairing interaction properly. We extend the ellipsoid contact like potential model (ECP), suitably modified and used previously by our group to model lipid bilayer phases with considerable success. This potential is used for base-base interactions, along with other potentials to capture bending, dihedral and solvent effects. The model shows a phase transition during hybridization and is able to reproduce the experimental melting curves with sufficient adequacy. Thermodynamical, along with conformational characteristics and structural properties of our model are studied in detail.

I. INTRODUCTION

DNA is one of the most important molecules, required for the propagation of life. Despite its apparent complex structure, it is built from chain of repeating units consisting of three main moieties, a phosphate group, a deoxyribose sugar, and one of four types of bases. The four bases, namely adenine, thymine, guanine and cytosine can be grouped into purines and pyrimidines based on their molecular structure. In standard DNA most commonly found in living cells, a purine molecule bound to a sugar backbone strand, takes part in hydrogen bonding interaction with a complementary pyrimidine [1]. Under normal conditions, this purine-pyrimidine binding is what gives double stranded DNA stability and their complementary nature ensures that replication of DNA is possible. This ability of replication and transcription of genetic information has made DNA a pivotal molecule for the growth of life. [2]. In recent times however, beyond its central biological role, DNA has also found applications in nanotechnology. The binding specificity of DNA which allows it to undergo sequence specific self-assembly, enables the design of nanoscale devices such as DNA tweezers [3]. Hence study of this elusive molecule warrants merit and has thus been the center of biological research for more than a century. Today, the chemical structure of DNA is more or less known, but to get a comprehensive picture of the structure property relationship important for biophysics and the related intermediate processes involved, requires us to resort to computer simulations. Additionally, to capture the structural and dynamical behavior of DNA in a reasonably expeditious way, computational models capable of balancing detail and efficacy are crucially needed [4].

Atomistic models simulated with force fields such as AMBER and CHARMM provide high accuracy but are limited to short time-scales, while continuum models sacrifice finer molecular detail. Coarse-grained (CG) simulations offer a middle ground, and numerous models—ranging from early one-dimensional lattice models of Peyrard and Bishop to more sophisticated models such as MARTINI for DNA have been developed to study DNA

mechanics and self-assembly [5]. The model of Peyrard and Bishop [6] is a simple one-dimensional model, with bases bound to its neighbors via harmonic springs. The bases were allowed one degree of freedom perpendicular to the springs, and interacted via a Morse potential with its minima at the zero of the coordinates. It was successful in replicating the dynamics of thermal denaturation of DNA and has been a topic of subsequent research. Later on, three dimensional CG models of DNA were developed to gain better insights on dynamical aspects. Maciejczyk et.al. [7] created a three-site model by considering a virtual atom for each of the three moieties of DNA and constructed a potential of mean force to define interparticle interactions for molecular simulation. The model was applied for the study of the transition between A and B forms of DNA. The popular oxDNA model by Ouldridge et.al. [8], the 3SPN model by Knotts et.al. [9] and its subsequent extensions [10] [11] and the MARTINI CG model extended to DNA [12] are popular coarse grained models extensively used for biophysical studies of DNA, and hence are part of molecular simulation packages. These models use spherical geometry for the bases with directionally modulated potentials to account for asymmetry in base interactions. Other models such as the model by Morris-Andrews et.al. [13] and Li et.al. [14] used ellipsoidal bases interacting via anisotropic Gaussian overlap potential (GOP) like potentials to better capture the planar geometry of the bases and their resulting interactions. Such potentials give an advantage over spherically symmetric potentials as the concept of orientation is woven into the mathematical form itself.

Since coarse graining is essentially a compromise over structural fidelity with computational limitations, not all coarse grained models can capture the significant characteristics of the biophysics of DNA. Essentially, coarse graining strategies are built around the particular phenomenon or interaction one wishes to study, and so better coarse graining strategies are always an active area of research. In this paper, we extend our earlier work with the ellipsoid contact type potential (ECP), originally applied for studying self-assembly of lipid bilayer phases [15] in a coarse grained model of DNA. The model potential is an extension of the ECP potential [16][17][18], which

is robust yet flexible enough to be applied to interactions between non-identical biaxial particles. The form of the potential is as given by Saha et.al. [19][20] with direction dependent energy scale correction. In the next section, we present the coarse-grained model of DNA used, analyze the resulting structures in the subsequent section, and discuss some future prospects.

II. MODEL

The potential model is composed of six terms. There exist two terms denoted by V_{bend} and $V_{dihedral}$ for the bonded interactions which account for the covalent structure of the molecule. The non-bonded interaction terms V_{ECP} and V_{solv} account for base pairing and implicit solvent interaction for renaturation of DNA. V_{exc} is the excluded volume interaction. Long range electrostatics is included via the term V_{el} . The terms are explained in more detail below.

$$V = V_{bend} + V_{dihedral} + V_{exc} + V_{el} + V_{ECP} + V_{solv}$$

The covalent bonding interactions are usually modeled by a harmonic or FENE spring. In our work, however, we do not consider that degree of freedom. We instead use hard constraint implemented via the RATTLE algorithm to constrain the bonds to their equilibrium distances. The order of magnitude for bond vibrational modes in real biomolecular systems is higher than bending vibrational modes, so it is a valid assumption to take it as a constant with respect to the slower bending and dihedral modes of the system.

The bending interaction is modeled as a harmonic interaction

$$V_{bend} = \sum_i^{angles} \frac{k_\theta}{2} (\theta_i - \theta_{0,i})^2 \quad (1)$$

Here, k_θ is the force constant which signifies how flexible the respective bond angle is about its equilibrium value of θ_0 . Torsional potential is included using a first order cosine form potential

$$V_{dihedral} = \sum_i^{dihedrals} \frac{k_\phi}{2} [1 - \cos(\phi_i - \phi_{0,i})] \quad (2)$$

where k_ϕ is the force constant of the dihedral degrees of freedom and ϕ_0 is the equilibrium angle. These represent the three and four body interactions which are critical for capturing the conformational flexibility of the DNA backbone. The bending potential is applied to the angle between sugar (S) position vectors and base (B) position vectors $v_{s1} = S_{i+1} - S_i$ and $v_{s2} = B_{i+1} - S_{i+1}$ for all $i = (1, N - 2)$. The dihedral potential is applied to the sugar base backbone. The three involved vectors for this

interaction are $v_{d1} = B_{i+1} - S_{i+1}$, $v_{d2} = S_{i+1} - S_i$ and $v_{d3} = S_i - B_i$. The dihedral angle is therefore given by

$$\cos \phi = \frac{(v_{d1} \times v_{d2}) \cdot (v_{d2} \times v_{d3})}{|v_{d1} \times v_{d2}| |v_{d2} \times v_{d3}|}$$

For both the bending and dihedral interaction, we set the equilibrium values at zero and the force constants at a low value. This is done to allow the system to find its own equilibrium configuration in the presence of other forces and excluded volume interaction, avoiding the introduction of any biases towards an intended configuration. Also since we study the renaturation of DNA by first heating the strands and then annealing, there is a high possibility of the strands getting stuck in *trans* like configurations, steering the system towards local minimas. The bending and dihedral modes serve to ensure that the angles in the system do not steer too far away from their initial values and destabilize the system, imparting structural rigidity to the single strands. The equations for the forces and torques for the bending and dihedral potential are available in standard textbooks on molecular simulation [21] [22].

V_{exc} is the excluded volume potential added to all the virtual particles in the model. For the bases having ellipsoidal geometry, the excluded volume is a sphere with radius equal to the semi-major axis of the ellipse. This excluded volume interaction is applied between all the different atoms except base base interactions, and between all atoms having direct constraints between them. In particular, for only interactions involving two bases, whether same strand or different, we use a separate V_{ECP} potential, the details of which shall be discussed shortly. The excluded volume interaction is represented by a repulsive Weeks-Chandler-Anderson (WCA) type potential of the following form

$$V_{exc} = \begin{cases} \sum_{i < j}^N \epsilon \left[\left(\frac{\sigma_e}{r} \right)^{12} - 2 \left(\frac{\sigma_e}{r} \right)^6 \right] + \epsilon, & (r \leq \sigma_e) \\ 0, & (r > \sigma_e) \end{cases} \quad (3)$$

where $\sigma_e = \frac{1}{2}[(\sigma_e)_i + (\sigma_e)_j]$ is the excluded volume diameter formed from the arithmetic mean of the excluded volume diameters of the interacting particles. The value of σ_e is different for each type of particle used in our simulation.

Long range electrostatics is modeled via the Debye Hückel term.

$$V_{el} = \sum_{i < j}^{N_s} \frac{q_i q_j}{4\pi\epsilon_0\epsilon_k r_{ij}} e^{r_{ij}/\kappa_D} \quad (4)$$

This term is an idealized approximation to model the non-ideal behavior of ionic solutions due to long range effects of electrostatic interactions. The potential is given

in the form of a Coulombic repulsion term modulated by an exponential decay, with a characteristic length scale κ_D known as the Debye length. The Debye length is dependent on the ionic strength I of the solution via the following relation

$$\kappa_D = \sqrt{\frac{\varepsilon_r \varepsilon_0 k_B T}{2 N_A e^2 I}} \quad (5)$$

Here ε_r is the dielectric constant of the solution, T is absolute temperature and e is the elementary charge unit. For physiological conditions of 100mM $[\text{Na}^+]$ solution, the Debye length is about 1 nm [23].

The next term is V_{solv} which is used to model the solvent interactions of the DNA backbone in an implicit manner. This term was taken by Sambriski et.al. [10] as an extension to the 3SPN.0 model force field to represent the many body effects associated with the solvent environment in an implicit manner. This avoids the calculation of solvent degrees of freedom which can account for up to half of simulation time. This term is added as an attractive interaction to the sugar atoms in the model.

$$V_{solv} = \sum_{i < j} \varepsilon_s \left[1 - e^{-\alpha(r_{ij} - r_0)} \right]^2 - \varepsilon_s \quad (6)$$

The solvent interaction term uses a Morse potential with interactions characterized by an interparticle separation term r_{ij} and energy scale ε_s which represents the dissociation energy or the well depth of the potential, and the equilibrium distance is represented by r_0 . For each of the n_s sugar atoms in one strand, the potential acts between itself and all the other sugar atoms in the opposite strand. For our simulation, we set the equilibrium distance at 20 Å which is the experimentally observed helix diameter for the B-DNA conformer. The width $\alpha = 5.333$ Å is same as in Ref [10] with $\varepsilon_s = 1.0$ taken for a reference solvent since in this work we do not study salt effects. This interaction strength should depend on the nature of the solvent environment for a more faithful representation.

The last term V_{ECP} is the potential that acts between the n_b base pairs in our model.. The bases in real DNA have planar ringed structures, whose interactions can be accurately captured by our ECP type model. To represent the potential, we start with the shifted form of the Lennard Jones potential given by

$$V_{ECP} = \epsilon \left[\left(\frac{\sigma_0}{r - \sigma + \sigma_0} \right)^{12} - \left(\frac{\sigma_0}{r - \sigma + \sigma_0} \right)^6 \right] \quad (7)$$

Here σ_0 controls the width of the LJ potential, r is the interparticle distance, σ is the distance of closest approach and ϵ is the respective energy well depth. For an ellipsoidal particle, the latter two quantities depend on both the orientations of the respective interacting parti-

cles and their direction of approach. The functional form we use for these terms is given by

$$\begin{aligned} \epsilon &= \epsilon_0 \epsilon_1^\nu(\hat{\alpha}, \hat{\beta}) \epsilon_2^\mu(\hat{\alpha}, \hat{\beta}, \hat{r}) \\ \sigma &= \sigma(\hat{\alpha}, \hat{\beta}, \hat{r}) \end{aligned}$$

Here $\hat{\alpha}$ and $\hat{\beta}$ are the respective orthogonal rotation matrices that define the orientation of the particle in the lab frame. The form of ϵ is similar to the form used in Gay-Berne potential [25]. The parameter values $\nu = 2$ and $\mu = 1$ are set as in Luckhurst et.al. [26]. The detailed form of the potential used, along with the expressions for the forces and torques are given in the appendix.

We also employ two additional modifications of the base potential form. First, we extend the range of the potential with a flat bottom part. The parameter that controls the width of this flat bottom region is given by ω_f . Let $\rho = \sigma_0/(r - \sigma + \sigma_0)$ be the dimensionless range parameter in the potential. Then

$$\rho = \begin{cases} \sigma_0/(r - \sigma + \sigma_0) & (r < \sigma_0) \\ 1 & (r \geq \sigma_0 \cap r \leq \omega_f \sigma_0) \\ \sigma_0/(r - \omega_f \sigma + \sigma_0) & (r \geq \omega_f \sigma_0) \end{cases}$$

The form of the potential for axial and transverse orientation of the two interacting ellipsoids is given in Figure 1. This potential acts as an attractive interaction between bases, which together with V_{solv} represents the implicit solvent in our model. Second, we separate the interaction potential into a pairing part and a stacking part. For each base on one strand, the pairing part han-

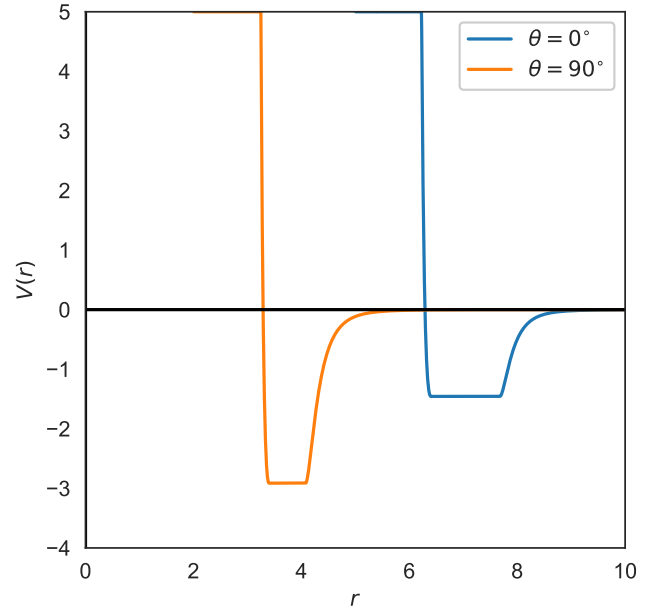


FIG. 1. Potential energy profiles for the flat bottom implicit solvent potential for side-side $\theta = 90^\circ$ and end-end configurations $\theta = 0^\circ$.

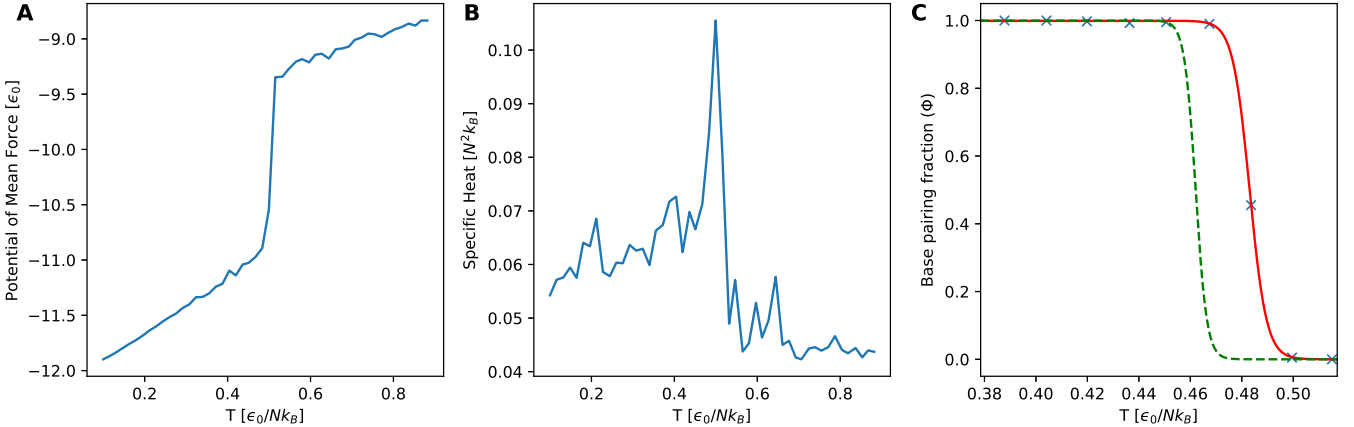


FIG. 2. Phase transition curves obtained from simulation. (A) Variation of the potential of mean force (PMF) with temperature. The jump at $T^* = 0.48$ indicates a phase change where ssDNA hybridizes into dsDNA. (B) Variation of specific heat capacity obtained from fluctuations in total energy $\langle \Delta E \rangle^2/T^{*2}$. Fluctuations are significantly higher around $T^* = 0.48$ where transition occurs in Fig A. (C) Melting curve obtained by fitting the sigmoid function given in Equation 8 over the pairing fraction Φ for each temperature. The crosses (\times) are actual data from simulation over which the sigmoid function is fitted. The dotted curve denotes a reference experimental curve taken from Ref [24] as mentioned in Section III C.

dles its interaction with all bases on the opposite strand. The stacking part, on the other hand, handles the interactions with its immediate neighbor bases above and below the concerned base on the same strand. Both these interactions have a cutoff and width parameter ω_f which we keep same for both parts at 50 Å and $1.2\sigma_0$ respectively.

The simulation is set up in Fortran 90 programming language. We initialize two strands of 20 bases each by placing them at lattice points. The bases are represented by uniaxial ellipsoids and all bases have identical geometries $(\sigma_x, \sigma_y, \sigma_z) = (2.0, 2.0, 1.0) \times 3.4$ Å and $(\epsilon_x, \epsilon_y, \epsilon_z) = (1.0, 1.0, 2.0) \times \epsilon_0$. Experimental free energies for stacking and pairing suggest a ratio of approximately 1.5 to 2 [27] [28]. The bond length between sugar atoms in the backbone is taken as 6.4 Å as discussed in Ref [8]. The bond length between sugar and base is taken as 6.4 Å. A harmonic flat bottom symmetric confinement potential with its zero at the center of the simulation box, is employed to constrain the center of mass of the two interacting strands from straying too far from each other during the simulation. The flat bottom potential has a radius of 50 Å. The strands do not feel any restorative force as long as the center of mass of the strands lie within the flat bottom part of the potential. Beyond that, the harmonic force pushes the strands towards the center. As the temperature is gradually reduced and bases start to pair, the confinement potential is ramped down to zero and the duplex is allowed to evolve freely. The restorative force from this potential is added to each particle equally, since all particles have unit reduced mass. This ensures no additional torques enter the system. The simulation was run in the NVT ensemble using Langevin stochastic thermostat. The strength of the damping term was set to 1.0 in units of inverse time. The thermostat used is coupled to both the translational and rotational degrees

of freedom.

Initially the two strands were kept separate from each other. We use the Velocity Verlet integrator to solve the translational motion. For rotational motion, quaternion algebra has been used. The rotational integrator is set up in a fashion similar to Velocity Verlet, following the scheme of Rozmanov et.al. [29]. The system was initially heated to $T^* = 0.9$ which took the system to a random configuration. After that we anneal the system in steps of $T^* = 0.02$ and each time equilibrate the system for 1×10^6 steps. The timestep for the simulation was set at around 0.005. The first 50% of the total time steps is used for equilibration. For the final 50% of time steps, we record the configuration state of the system every 5000 steps. The values of the potential and total energy of the system are also recorded for each timestep during the final 50% timesteps.

III. RESULTS

Coarse-graining (CG) by definition is a systematic dimensionality reduction technique that maps a high-dimensional atomistic system onto a simplified representation with fewer degrees of freedom. This increases computational efficiency while still preserving essential thermodynamic behavior. Let \vec{x} and \vec{X} define the atomistic and CG coordinates respectively. We can define a mapping $\mathcal{M} : \vec{x} \rightarrow \vec{X}$ which maps atomistic system configurations to CG coordinate configurations. Then the potential of mean force (PMF) represents the ratio of free energy of all the configurations that map to a CG coordinate R , relative to the total free energy of the atomistic system. In essence it is the free energy computed over the marginal probability distribution of configurations in

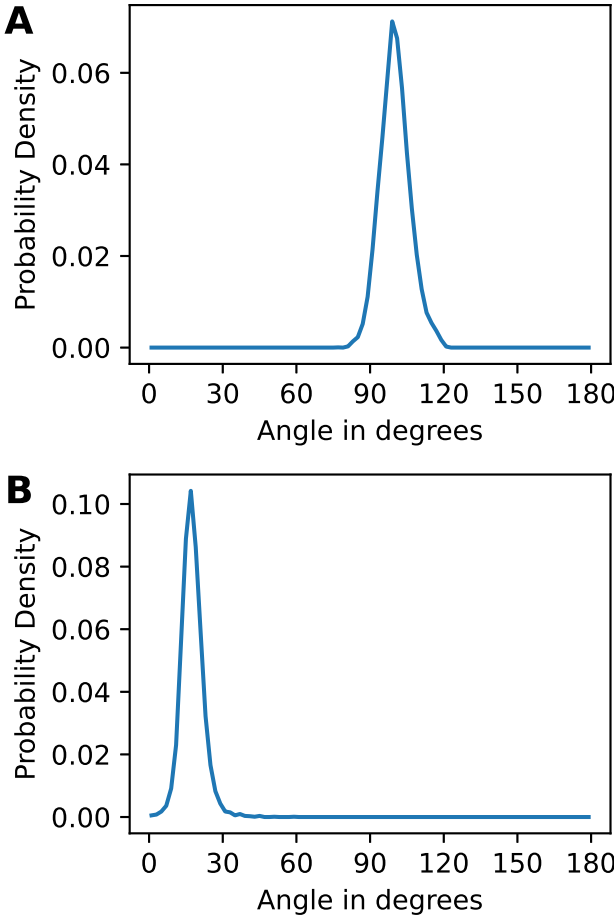


FIG. 3. (A) Bending angle distribution. (B) Dihedral angle distribution. Both distributions settle at equilibrium value with peaks at 99° and 17° respectively as the system cools towards hybridized state.

the CG variable \vec{X} , the actual configurations being integrated out according to the mapping \mathcal{M} . Since we are mainly interested in free energy differences, phase behavior of the system can be categorized on the basis of nature of PMF at different temperatures.

For our model, we first construct the potential of mean force $V(\vec{X})$ in CG coordinates defining interparticle interactions under which the system evolves and track the variation of the potential from simulation outputs. In Figure 2A, we plot the potential of mean force with corresponding reduced system temperature. For each temperature, we store the PMF values for the last 50% steps (after the system has adequately equilibrated) and report the mean value. We obtain a first-order like jump in the graph. The corresponding mean squared fluctuation in the total energy function $\langle \Delta E^2 \rangle$ divided by the square of system temperature gives us the variation of specific heat C_V which is plotted in Figure 2B. This graph too gives a peak around $T^* = 0.5 \epsilon_0 / N k_B$ indicating a phase change in the system.

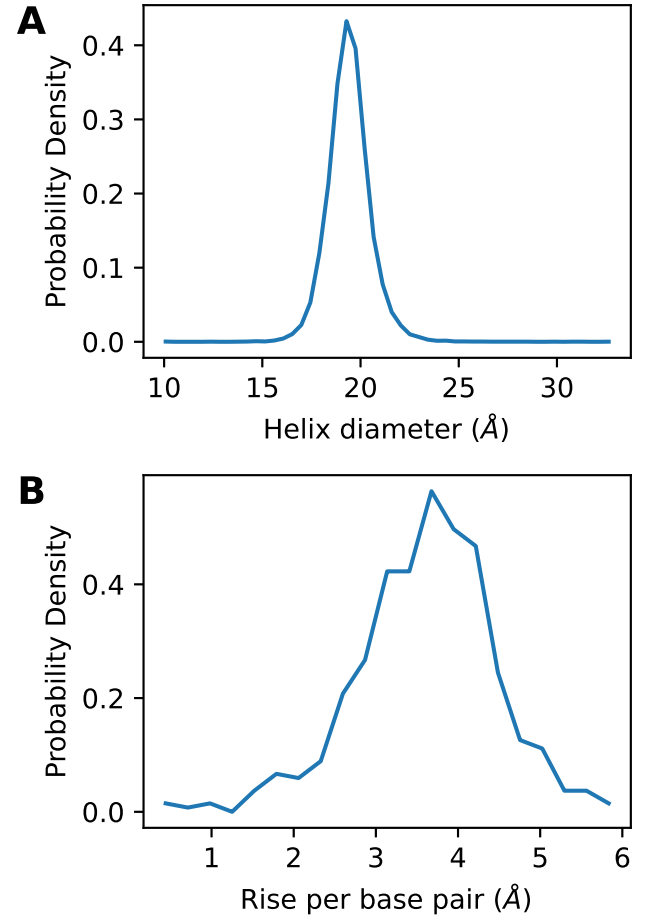


FIG. 4. (A) Estimate of the helix diameter from model simulation. (B) Average rise per base pair obtained by calculating the local helical axis using the scheme described in Section III B. The local helical axis is given by the principal component of the covariance matrix formed from the base centers around the bases being probed. Estimated value from graph is around 3.677 \AA

We can also find the melting temperature from the fraction of paired bases formed, also termed the pairing fraction (Φ). For this we treat bases as paired if the distance between them is less than 12 \AA . We then fit a sigmoid curve over the data. The form of the sigmoid function is taken as

$$f(x) = \frac{a}{1 + e^{-b(x-x_0)}} \quad (8)$$

The best fit is found from the data and the melting curve is obtained. Using the temperature scaling parameter value, the transition point is obtained at $T^* = 0.483 \epsilon_0 / N k_B$. Figure 2C plots the respective melting profiles for both the simulation and experimental melting curve.

In Figure 3, we plot the bending and dihedral distribution obtained from our model. The obtained maxima value for bending angle is at $\theta = 99^\circ$ and for dihedral

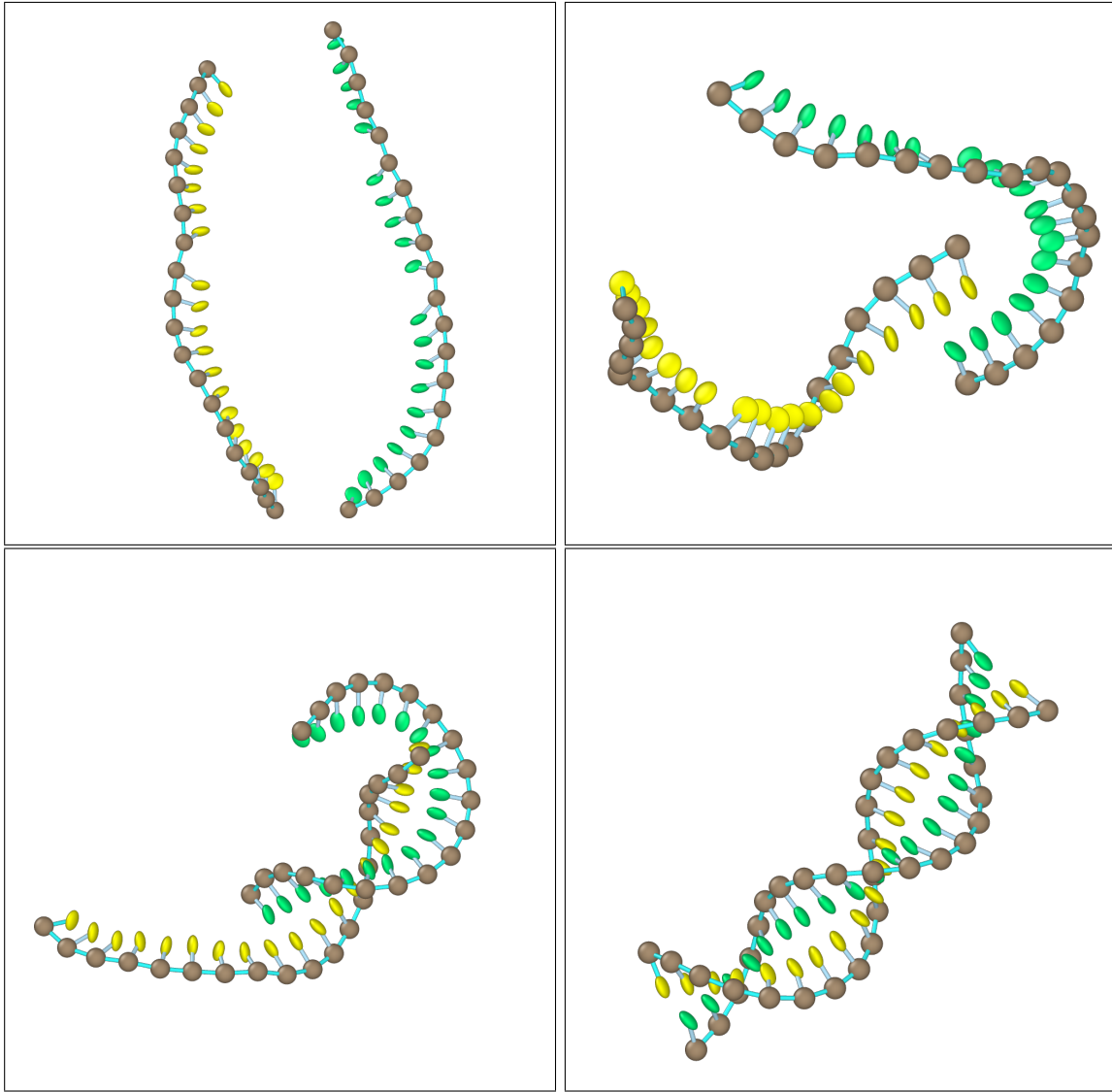


FIG. 5. Snapshots from the simulation. The particle sizes are slightly reduced to enhance visual clarity. (A) Initially the two chains are separate from each other. The system is heated well to ensure a random starting configuration of position and orientation. (B) As the system is cooled beyond the transition point, the bases begin binding with their complementary counterparts. Here the first binding event occurs between the bases on opposite strands. As can be seen, hybridization starts at one end and moves forward from there. (C) The strands slide forward along the bases of its complementary strand. This is feasible since in our model, base pairing lowers free energy. (D) Finally, as all bases pair successfully, the strands hybridize into a double helix structure.

is at $\phi = 17^\circ$. In Figure 4A, we plot the obtained helix diameter from simulations at 20 Å. We also plot the distribution of average rise per base pair from our model in Figure 4B. To obtain it, we first construct a local helix axis around the bases being probed in the range of 3 bp. For example, let's say we want to find the rise between base index i and $i + 1$. So, we construct the local helix axis from base centers $i - 3$ to $i + 3$. The coordinates of the base centers are used to construct a local covariance matrix. The helix axis is obtained via principal component analysis (PCA), which is the eigenvector corresponding to the largest eigenvalue of the covariance

matrix. The vector difference in positions $d_1 = B_{i+1} - B_i$ is projected onto the local helical axis to obtain the rise for bases B_i and B_{i+1} . This distance averaged for all bases (excluding three bases from both ends) gives us the average rise per base pair. We deliberately leave out three bases from both ends for this analysis since they display fraying which can give incorrect results. The estimated value from the graph is 3.677 Å which is close to the experimentally reported value of 3.4 Å [30] [31].

All values and their magnitudes reported here are in reduced coordinates. In this section we provide the equivalent real world values. All our length magnitudes are re-

ported in Angstroms directly since we chose 1 Å as unit of length. For reporting the energy scale, we choose a uniform scaling factor ϵ_0 so as to match the pairing energy of simulation with experimentally obtained pairing free energies [27]. We set its value at $\epsilon_0 = 6.0$ kJ/mol. The conversion to equivalent real system temperature unit follows the equation

$$T^* = \frac{N_A k_B T}{\epsilon_0} \quad (9)$$

Where N_A is the Avogadro number and k_B is the Boltzmann constant and ϵ_0 is a constant energy scale. Also, since we cannot match simulated melting temperatures to their experimental counterparts for specific sequences or salt concentrations, our results stated here are only approximately true. Owczarzy et.al. [24] provides a comprehensive list of melting temperatures of DNA sequences of varying length, sequence and salt concentrations. We take one such sequence as a reference, the 20-mer TACTTCCAGTGCTCAGCGTA at 69mM [Na⁺], which has a melting temperature of 333.45 K. This is indicated by the dotted line in Figure 2C. Applying the temperature conversion formula and the energy scale, $T^* = 0.483$ corresponds to $T = 348.58$ K.

IV. CONCLUSION

In this paper, we extend our ECP like potential [19] in a coarse-grained model of DNA and tally them with experimental data to assess the significance of our model to predict DNA biophysics. The potential model is applied for base base interactions. For different base pairs, shape anisotropies are not same. This is true for energy parameters as well. Gaussian overlap type potentials (GOP) like Gay-Berne potential, though widely used, are incapable of handling a system of non-identical species having ellipsoidal anisotropy accurately. In DNA, purine interacts with pyrimidines during pairing. Purines have different shape and energy anisotropies in comparison with pyrimidines. Again, an A-T pair is different from a G-C pair. ECP type potential which can take into account these features are most suitable for studying base pairing interaction in DNA. We separate the inter-strand base pairing interactions from intra-strand stacking interactions. This facilitates dsDNA formation by avoiding hairpin configurations. For the bonded interactions we stick to standard harmonic and cosine potentials for bending and dihedral

interactions respectively. The bonds use hard constraints implemented via RATTLE algorithm. An excluded volume WCA potential is applied to prevent atoms from overlapping, the radius of exclusion sphere taken different for each type of particle. We introduce implicit solvent effects via a Morse potential and a flat bottom part in our ECP like potential. Electrostatics is considered using Debye Huckel approximation. Since it is valid in the limit of high salt concentration, our model cannot yet provide an approximation for the low salt regime. However for physiological conditions, the approximation is valid enough.

Our model is simulated using in house code written in Fortran 90, where the bases are annealed from a random configuration at high temperature to a minimum energy configuration at low temperature. The melting profiles obtained are compared with reference experimental melting profiles with a suitably considered energy scale. Satisfactory agreement is obtained with experimental values considering the simplistic nature of our model. We also provide snapshots of the simulation to elucidate the annealing process.

For our future work, we attempt to find a suitable potential form to simulate the formation of grooves. Much about the structure of grooves, the factors that contribute to its size and its conformational effects still remain to be well understood. How angular deformations can deform the DNA groove stability and contribute to malignancy in the cell, are active research questions we seek to probe. We also intend to study the effect of salt concentration on renaturation and denaturation of DNA. These are areas currently being pursued in our lab. Nevertheless, we hope our model is helpful in future work regarding DNA biophysics and DNA-protein or DNA-lipid interactions.

ACKNOWLEDGMENTS

This research was funded by the Council of Scientific and Industrial Research with grant number (09/0028(19444)/2024-EMR-I). Computational resources were provided by the University of Calcutta. OpenMP was used for code parallelization. The software OVITO was used for visualizations. The graphs were plotted in the Python programming language using the matplotlib plotting library.

[1] W. Saenger, *Principles of nucleic acid structure*, [4. aufl.] ed., Springer advanced texts in chemistry (Springer, New York, 1995) literaturverz. S. 459 - 540.

[2] G. Ferry, The structure of dna, *Nature* **575**, 35 (2019).

[3] N. C. Seeman and H. F. Sleiman, Dna nanotechnology, *Nature Reviews Materials* **3**, 10.1038/natrevmats.2017.68 (2017).

[4] Z.-C. Mu, Y.-L. Tan, J. Liu, B.-G. Zhang, and Y.-Z. Shi, Computational modeling of dna 3d structures: From dynamics and mechanics to folding, *Molecules* **28**, 4833 (2023).

[5] H. I. Ingólfsson, C. A. Lopez, J. J. Uusitalo, D. H.

de Jong, S. M. Gopal, X. Periole, and S. J. Marrink, The power of coarse graining in biomolecular simulations, *WIREs Computational Molecular Science* **4**, 225 (2013).

[6] M. Peyrard, Nonlinear dynamics and statistical physics of dna, *Nonlinearity* **17**, R1 (2004).

[7] M. Maciejczyk, W. R. Rudnicki, and B. Lesyng, A mesoscopic model of nucleic acids. part 2. an effective potential energy function for dna, *Journal of Biomolecular Structure and Dynamics* **17**, 1109 (2000).

[8] T. E. Ouldridge, A. A. Louis, and J. P. K. Doye, Structural, mechanical, and thermodynamic properties of a coarse-grained dna model, *The Journal of Chemical Physics* **134**, 10.1063/1.3552946 (2011).

[9] T. A. Knotts, N. Rathore, D. C. Schwartz, and J. J. de Pablo, A coarse grain model for dna, *The Journal of Chemical Physics* **126**, 10.1063/1.2431804 (2007).

[10] E. Sambriski, D. Schwartz, and J. de Pablo, A mesoscale model of dna and its renaturation, *Biophysical Journal* **96**, 1675 (2009).

[11] D. M. Hinckley, G. S. Freeman, J. K. Whitmer, and J. J. de Pablo, An experimentally-informed coarse-grained 3-site-per-nucleotide model of dna: Structure, thermodynamics, and dynamics of hybridization, *The Journal of Chemical Physics* **139**, 10.1063/1.4822042 (2013).

[12] J. J. Uusitalo, H. I. Ingólfsson, P. Akhshi, D. P. Tielemans, and S. J. Marrink, Martini coarse-grained force field: Extension to dna, *Journal of Chemical Theory and Computation* **11**, 3932 (2015).

[13] A. Morris-Andrews, J. Rottler, and S. S. Plotkin, A systematically coarse-grained model for dna and its predictions for persistence length, stacking, twist, and chirality, *The Journal of Chemical Physics* **132**, 10.1063/1.3269994 (2010).

[14] G. Li, H. Shen, D. Zhang, Y. Li, and H. Wang, Coarse-grained modeling of nucleic acids using anisotropic gay-berne and electric multipole potentials, *Journal of Chemical Theory and Computation* **12**, 676 (2016).

[15] S. Bhowmick and J. Saha, Coarse-grained solvent-free model for computer simulation of self-assembled amphiphiles, *Scientific Reports* **15**, 10.1038/s41598-025-24277-0 (2025).

[16] J. W. Perram, J. Rasmussen, E. Præstgaard, and J. L. Lebowitz, Ellipsoid contact potential: Theory and relation to overlap potentials, *Physical Review E* **54**, 6565 (1996).

[17] L. Paramonov and S. N. Yaliraki, The directional contact distance of two ellipsoids: Coarse-grained potentials for anisotropic interactions, *The Journal of Chemical Physics* **123**, 10.1063/1.2102897 (2005).

[18] G. Ayton and G. N. Patey, A generalized gaussian overlap model for fluids of anisotropic particles, *The Journal of Chemical Physics* **102**, 9040 (1995).

[19] J. Saha, Study of liquid crystal phases with a model soft ellipsoid contact potential, *Physics Letters A* **375**, 1893 (2011).

[20] J. Saha, Soft ellipsoid potential for biaxial molecules, *Molecular Simulation* **42**, 1437 (2016).

[21] M. P. Allen and D. J. Tildesley, *Computer simulation of liquids*, second edition ed. (Oxford University Press, Oxford, 2017).

[22] D. C. Rapaport, *The art of molecular dynamics simulation*, 2nd ed. (Cambridge Univ. Press, Cambridge [u.a.], 2010).

[23] J. G. Hedley, K. Coshic, A. Aksimentiev, and A. A. Kornyshev, Electric field of dna in solution: Who is in charge?, *Physical Review X* **14**, 031042 (2024).

[24] R. Owczarzy, Y. You, B. G. Moreira, J. A. Manthey, L. Huang, M. A. Behlke, and J. A. Walder, Effects of sodium ions on dna duplex oligomers: Improved predictions of melting temperatures, *Biochemistry* **43**, 3537 (2004).

[25] J. G. Gay and B. J. Berne, Modification of the overlap potential to mimic a linear site-site potential, *The Journal of Chemical Physics* **74**, 3316 (1981).

[26] G. R. Luckhurst, R. A. Stephens, and R. W. Phippen, Computer simulation studies of anisotropic systems. xix. mesophases formed by the gay-berne model mesogen, *Liquid Crystals* **8**, 451 (1990).

[27] P. L. Privalov and C. Crane-Robinson, Forces maintaining the dna double helix, *European Biophysics Journal* **49**, 315 (2020).

[28] J. Abraham Punnoose, K. J. Thomas, A. R. Chandrasekaran, J. Vilcapoma, A. Hayden, K. Kilpatrick, S. Vangaveti, A. Chen, T. Banco, and K. Halvorsen, High-throughput single-molecule quantification of individual base stacking energies in nucleic acids, *Nature Communications* **14**, 10.1038/s41467-023-36373-8 (2023).

[29] D. Rozmanov and P. G. Kusalik, Robust rotational-velocity-verlet integration methods, *Physical Review E* **81**, 056706 (2010).

[30] S. Arnott, R. Chandrasekaran, D. L. Birdsall, A. G. W. Leslie, and R. L. Ratliff, Left-handed dna helices, *Nature* **283**, 743 (1980).

[31] R. Langridge, H. Wilson, C. Hooper, M. Wilkins, and L. Hamilton, The molecular configuration of deoxyribonucleic acid, *Journal of Molecular Biology* **2**, 19 (1960).

[32] R. P. Brent, *Algorithms for minimization without derivatives*, @Prentice-Hall series in automatic computation (Prentice-Hall, Englewood Cliffs, N.J., 1973).

[33] R. Berardi, C. Fava, and C. Zannoni, A generalized gay-berne intermolecular potential for biaxial particles, *Chemical Physics Letters* **236**, 462 (1995).

[34] M. P. Allen and G. Germano, Expressions for forces and torques in molecular simulations using rigid bodies, *Molecular Physics* **104**, 3225 (2006).

Appendix: Our ECP like potential

The potential equation for ECP is similar to that of Gay Berne, given by

$$U_{GB}(\vec{r}, \hat{\alpha}, \hat{\beta}) = 4 \epsilon_0 \epsilon_1^\nu(\hat{\alpha}, \hat{\beta}) \epsilon_2^\mu(\hat{\alpha}, \hat{\beta}, \hat{r}) \left[\left(\frac{\sigma_0}{r - \sigma(\hat{\alpha}, \hat{\beta}, \hat{r}) + \sigma_0} \right)^{12} - \left(\frac{\sigma_0}{r - \sigma(\hat{\alpha}, \hat{\beta}, \hat{r}) + \sigma_0} \right)^6 \right]$$

The orthogonal rotation matrices $\hat{\alpha}$ and $\hat{\beta}$ are obtained from the respective rotation quaternion associated with each of the two interacting ellipsoids that we use in our simulation. Since the potential is a pair potential, we represent the two particles using shape matrices S_1 and S_2 given by

$$S_1 = \begin{pmatrix} \sigma_{1_x} & 0 & 0 \\ 0 & \sigma_{1_y} & 0 \\ 0 & 0 & \sigma_{1_z} \end{pmatrix}; \quad S_2 = \begin{pmatrix} \sigma_{2_x} & 0 & 0 \\ 0 & \sigma_{2_y} & 0 \\ 0 & 0 & \sigma_{2_z} \end{pmatrix}$$

This defines the geometry of the particles in the molecular frame. To represent the rotation of the particle, we convert the shape matrix from molecular frame into the lab frame to obtain matrices A and B given by

$$A = \hat{\alpha}^T S_1^2 \hat{\alpha}$$

$$B = \hat{\beta}^T S_2^2 \hat{\beta}$$

The matrices A and B now encompass the orientational geometry of the ellipsoids. The point of contact must lie on a line of position vectors \vec{r} satisfying $A(\vec{r}) = B(\vec{r})$ where $A(\vec{r}) = (\vec{r} - \vec{r}_A)^T A (\vec{r} - \vec{r}_A)$ and $B(\vec{r}) = (\vec{r} - \vec{r}_B)^T B (\vec{r} - \vec{r}_B)$, \vec{r}_A and \vec{r}_B being the respective ellipsoid centers. The contact vector must also lie on the surface of the respective ellipsoids which means it must satisfy both $A(\vec{r}) = 1$ and $B(\vec{r}) = 1$. To find the contact point systematically, a parametric function of both ellipses φ is constructed whose form is given by

$$\varphi = \lambda_D (1 - \lambda_D) \hat{r} [(1 - \lambda_D) A + \lambda_D B]^{-1} \hat{r}$$

Where $r = \vec{r}_A - \vec{r}_B$ signifies the direction of approach. This now becomes an optimization problem. The point of contact can be found out from the value of λ_D that maximizes the function φ . However, the actual point of contact \vec{r} is of little interest, since whether the spheres are in contact or for away can be inferred from the value of φ at the stationary point itself. The shift term is then given by

$$\sigma^{-2} = \varphi = \lambda_D (1 - \lambda_D) \hat{r} [(1 - \lambda_D) A + \lambda_D B]^{-1} \hat{r}$$

All that is left is to construct the function φ itself and find its stationary point using optimization algorithms such as Brent's method [32].

The energy ϵ consists of three terms ϵ_0 , ϵ_1 and ϵ_2 . We set $\epsilon_0 = \min(\epsilon_x, \epsilon_y, \epsilon_z)$. For $\epsilon_1(\alpha, \beta)$ we use the formula given by Berardi et al [33]

$$\epsilon_1(\alpha, \beta) = \frac{(\sigma_x \sigma_y + \sigma_z^2)}{8} \sqrt{2 \sigma_x \sigma_y \det(E)}$$

where $E = A + B$. In short we can write it as $\epsilon_1 = \sigma_t \sqrt{\det(E)}$ where σ_t now replaces the constant coefficient. Since σ_t is a function of the geometry of any one ellipse, we take the geometric mean $\sigma_t = \sqrt{\sigma_{t_1} \sigma_{t_2}}$. This is necessary since for the general case the geometries of A and B need not be similar, which is the case for mixtures.

The term ϵ_2 depends not only on the orientation but on the inter center distance r . We calculate it similar to the way we calculate σ with slight modifications. The energy matrices F_1 and F_2 in the molecular frame is given by

$$F_1 = \begin{pmatrix} \left(\frac{\epsilon_0}{\epsilon_{1_x}} \right)^{1/\mu} & 0 & 0 \\ 0 & \left(\frac{\epsilon_0}{\epsilon_{1_y}} \right)^{1/\mu} & 0 \\ 0 & 0 & \left(\frac{\epsilon_0}{\epsilon_{1_z}} \right)^{1/\mu} \end{pmatrix}; \quad F_2 = \begin{pmatrix} \left(\frac{\epsilon_0}{\epsilon_{2_x}} \right)^{1/\mu} & 0 & 0 \\ 0 & \left(\frac{\epsilon_0}{\epsilon_{2_y}} \right)^{1/\mu} & 0 \\ 0 & 0 & \left(\frac{\epsilon_0}{\epsilon_{2_z}} \right)^{1/\mu} \end{pmatrix}$$

As before, we convert the diagonal matrices from the molecular frame to the lab frame to obtain matrices M and N

which represent the orientation dependent energy strength

$$M = \hat{\alpha}^T F_1 \hat{\alpha}$$

$$N = \hat{\beta}^T F_2 \hat{\beta}$$

Similar to the case of φ , we construct an optimization problem for the function ϱ with parameter λ_E . The stationary point gives us the energy scale of the potential in the respective direction.

$$\epsilon_2 = \varrho = \lambda_E (1 - \lambda_E) \hat{r} [(1 - \lambda_E) M + \lambda_E N]^{-1} \hat{r}$$

This potential form accurately represents geometry of ellipsoidal molecules, contrary to the Gay Berne implementation.

The forces and torques for the distance dependent part of a general ellipsoid contact potential is given by Allen et.al. [34]. Here we write the expressions for the forces and torques for our ECP like potential model as given in Saha et.al. [19]. Let $G = [(1 - \lambda_D)A + \lambda_D B]$. Then we can write the above equation in a more compact form

$$\psi = \lambda_D (1 - \lambda_D) \hat{r} \cdot G^{-1} \cdot \hat{r}$$

If we also assume $\vec{k} = G^{-1} \hat{r}$ such that \vec{k} the solution of a linear equation $G \cdot \vec{k} = \hat{r}$, then we can write the derivative of φ with respect to \hat{r} in terms of k . It is given by

$$\frac{\partial \varphi}{\partial \hat{r}} = 2\lambda_D (1 - \lambda_D) \frac{\vec{k}}{r}$$

The derivative for the term ϱ has the same mathematical form as that of φ with λ_D replaced by λ_E and \vec{k} replaced by \vec{k}_E . With this we can write the equation of the interparticle force, which is

$$F = \epsilon_1^\nu \mu \epsilon_2^{\mu-1} [\rho^{-12} - \rho^{-6}] \frac{2\lambda_E (1 - \lambda_E)}{r^2} [\vec{k}_E - (\vec{k}_E \cdot \hat{r}) \hat{r}]$$

$$+ \epsilon_1^\nu \epsilon_2^\mu [6\rho^{-7} - 12\rho^{-13}] \left(\frac{\vec{r}}{\sigma_0 r} + \frac{2\lambda_D (1 - \lambda_D)}{2\sigma_0 r^2} \varphi^{-\frac{3}{2}} [\vec{k} - (\vec{k} \cdot \hat{r}) \hat{r}] \right)$$

We also give the equations for the torques acting on the ellipsoids, incorporating the derivative of ϵ_1 with respect to $\hat{\alpha}$ and $\hat{\beta}$ into the respective equation

$$\tau_1 = \nu \epsilon_1^{\nu-1} \epsilon_2^\mu [\rho^{-12} - \rho^{-6}] \sum_m [a_m \times E^{-1} \cdot a_m]$$

$$+ \epsilon_1^\nu \mu \epsilon_2^{\mu-1} [\rho^{-12} - \rho^{-6}] \frac{2\lambda_E (1 - \lambda_E)^2}{r^2} [\vec{k}_E \cdot M \times \vec{k}_E]$$

$$+ \epsilon_1^\nu \epsilon_2^\mu [6\rho^{-7} - 12\rho^{-13}] \left(\frac{2\lambda_D (1 - \lambda_D)^2}{2\sigma_0 r^2} \varphi^{-\frac{3}{2}} [\vec{k} \cdot A \times \vec{k}] \right)$$

and

$$\tau_2 = \nu \epsilon_1^{\nu-1} \epsilon_2^\mu [\rho^{-12} - \rho^{-6}] \sum_m [b_m \times E^{-1} \cdot b_m]$$

$$+ \epsilon_1^\nu \mu \epsilon_2^{\mu-1} [\rho^{-12} - \rho^{-6}] \frac{2\lambda_E^2 (1 - \lambda_E)}{r^2} [\vec{k}_E \cdot N \times \vec{k}_E]$$

$$+ \epsilon_1^\nu \epsilon_2^\mu [6\rho^{-7} - 12\rho^{-13}] \left(\frac{2\lambda_D^2 (1 - \lambda_D)}{2\sigma_0 r^2} \varphi^{-\frac{3}{2}} [\vec{k} \cdot B \times \vec{k}] \right)$$

where $\epsilon : E^{-1} A = \sum_m [a_m \times E^{-1} \cdot a_m]$ and a_m are the rows of the matrix $\hat{\alpha} S_1$. A similar equation is obtained for the matrix B .
